ResearchGate

See discussions, stats, and author profiles for this publication at: https://www.researchgate.net/publication/38042243

Amyloid-Like Self-Assembly of Peptide Sequences from the Adenovirus Fiber Shaft: Insights from Molecular Dynamics Simulations

ARTICLE *in* THE JOURNAL OF PHYSICAL CHEMISTRY B · OCTOBER 2009

Impact Factor: 3.3 · DOI: 10.1021/jp9066718 · Source: PubMed

CITATIONS
21

READS
25

4 AUTHORS, INCLUDING:

Phanourios Tamamis
Princeton University
26 PUBLICATIONS **248** CITATIONS
SEE PROFILE

Emmanouil Kasotakis
National University of Ireland, Galway
19 PUBLICATIONS **219** CITATIONS
SEE PROFILE

Anna Mitraki
University of Crete
58 PUBLICATIONS **1,791** CITATIONS
SEE PROFILE

Available from: Phanourios Tamamis
Retrieved on: 26 January 2016

Amyloid-Like Self-Assembly of Peptide Sequences from the Adenovirus Fiber Shaft: Insights from Molecular Dynamics Simulations

Phanourios Tamamis,[†] Emmanouil Kasotakis,[‡] Anna Mitraki,[‡] and Georgios Archontis*[,†]

Department of Physics, University of Cyprus, PO20537, CY1678 Nicosia, Cyprus, and Department of Materials Science and Technology, University of Crete, and Institute for Electronic Structure and Laser, FORTH, Heraklion, Crete, Greece

Received: July 15, 2009; Revised Manuscript Received: October 6, 2009

The self-assembly of peptides and proteins into nanostructures is related to the fundamental problems of protein folding and misfolding and has potential applications in medicine, materials science and nanotechnology. Natural peptides, corresponding to sequence repeats from self-assembling proteins, may constitute elementary building blocks of such nanostructures. In this work, we study by implicit-solvent replica-exchange simulations the self-assembly of two amyloidogenic sequences derived from the naturally occurring fiber shaft of the adenovirus, the octapeptide NSGAITIG (asparagine-serine-glycine-alanine-isoleucine-threonine-isoleucine-glycine) and its hexapeptide counterpart, GAITIG. In accordance with their amyloidogenic capacity, both peptides form readily intermolecular β-sheets, stabilized by extensive main- and side-chain contacts involving the C-terminal moieties (segments 3−8 and 2−6, respectively). The structural and energetic properties of these sheets are analyzed extensively. The N-terminal residues Asn1 and Ser2 of the octapeptide remain disordered in the sheets, suggesting that these residues are exposed at the exterior of the fibrils and accessible. On the basis of insight provided by the simulations, cysteine residues were recently substituted at positions 1 and 2 of NSGAITIG; the newly designed peptides maintain their amyloidogenic properties and can bind to silver, gold and platinum nanoparticles [Kasotakis et al. *Biopolymers* **2009**, *92*, 164−172]. Computational investigation can identify suitable positions for rational modification of peptide building blocks, aiming at the fabrication of novel biomaterials.

1. Introduction

The self-assembly of proteins and peptides into amyloid fibers,[1−4] nanostructures of various morphologies,[5−7] and systems responsive to external stimuli[6,8] is the focus of extensive experimental[1−13] and computational studies,[11,13−25] as it is related to the fundamental problems of biomolecular folding and association and has potential applications in medicine, nanotechnology, and materials science. In the work presented here, we study by computational methods the self-assembly of short peptide sequences derived from the adenovirus fiber shaft.

The adenovirus type-2 fibers are homotrimeric, 582-residue proteins, consisting of a virus-binding N-terminal tail, a central shaft with repeating sequence motifs, and a globular, receptor-binding C-terminal domain (reviewed in Mitraki et al.[26]). Crystallographic studies of a stable trimeric domain (residues 319−582), containing four repeats of the adenovirus type-2 fiber shaft and the receptor-binding head have shown that the trimer folds into a novel triple β-spiral fold.[27] The formation of the fold requires the individual monomers to be brought into correct register. This is achieved by the C-terminal head domain,[28] but can also be accomplished by some other registration agent, such as the trimerization domain of the bacteriophage T4 fibritin.[29] In contrast, sequence segments from the adenovirus shaft aggregate under physiological conditions into amyloid-like fibrils. This was demonstrated for five peptides with lengths of 6, 8, 12, 25, and 41 residues by Congo red binding, electron microscopy, infrared spectroscopy and X-ray fiber diffraction methods.[9,30]

Here we focus on the two shortest peptides studied in Papanikolopoulou et al.,[9] the octapeptide NSGAITIG and the hexapeptide GAITIG. The NSGAITIG sequence is a part of a 15-residue repeating motif in the fiber shaft. The residues N-S-G fold into a type-II turn and the residues A-I-T-I-G constitute part of a β-strand, which forms several hydrogen-bonding interactions within the same monomer and with one adjacent monomer in the trimeric shaft. Residues I5 and I7 correspond to conserved apolar positions, which contribute to the central hydrophobic core of the shaft.

The participation of NSGAITIG and GAITIG in the sequence repeat of the fiber shaft suggests that these peptides are elementary self-assembling building blocks, as confirmed in Papanikolopoulou et al.[9] The conformations of the NSGAITIG and GAITIG peptides are not known in their respective amyloid fibers, or in solution. In order to obtain a better understanding of the structural and energetic properties of the fibers formed by these peptide sequences, we perform molecular dynamics simulations of aqueous solutions containing multiple copies of the two peptides, with a replica-exchange method[31−36] in implicit solvent.[37] The simulations show that both peptides have a high propensity to aggregate into intermolecular conformations with β-sheet content, in accordance with their amyloidogenic capacity. These conformations are stabilized by extensive main- and side-chain contacts, involving the segments 3−8 and 2−6, respectively, in the octapeptide and hexapeptide oligomers. The N-terminal residues of the octapeptide (Asn1 and Ser2) do not participate in the β-sheet conformations observed in the simula-

* Corresponding author. Tel: +357 22 89 28 22. Fax: +357 22 89 28 21. E-mail: archonti@ucy.ac.cy.
[†] University of Cyprus.
[‡] University of Crete, and Institute for Electronic Structure and Laser, FORTH.

10.1021/jp9066718 CCC: $40.75 © 2009 American Chemical Society
Published on Web 10/29/2009

tions. Thus, it is possible that they are not engaged in the cross-beta core within the fibrils, but are exposed at the exterior of the fibril and accessible. In accord with the simulations, cysteine residues were recently substituted at positions 1 and 2; the newly designed peptides formed amyloid fibrils capable of binding to silver, gold and platinum nanoparticles, confirming the accessibility of the residues at these positions.[38] Such metal-binding peptides, with self-assembling properties, may have a potential use as conducting nanowires, with applications in nanocircuitry.

The next section describes the simulation systems and the methods employed in the analysis. Results are presented next; the last section is a discussion.

2. Methods

Systems. In the octapeptide simulations, the system consisted of three monomers with the sequence NH_3^+-NSGAITIG-NH_2. In the hexapeptide simulations, the system contained six monomers with the sequence NH_3^+-GAITIG-NH_2. The terminal groups were chosen for consistency with the experimental sequences.

Force Field. The peptide atomic charges, van der Waals and stereochemical parameters were taken from the CHARMM22 all-atom force field.[39] Solvent effects were taken into account implicitly by the recent (C22) implicit solvent model FACTS of Caflisch;[37] a dielectric constant $\varepsilon = 1$ was assigned to the peptide. The nonpolar solvation energy was proportional to the solvent-exposed surface area, with a surface-tension proportionality coefficient of 0.015 kcal/mol/Å^2. A 12 Å cutoff was used for the nonbonded interactions, for consistency with the FACTS parametrization.[37] The equations of motion were integrated by the leapfrog algorithm, with a 2.0 fs time step. Bonds involving hydrogen atoms were constrained to standard values with the SHAKE algorithm,[40] as implemented into the CHARMM program.[41] The temperature was controlled by the Langevin method; the friction coefficients were set to 5.0 ps^{-1} for heavy atoms and 0 ps^{-1} for hydrogen atoms. In the NSGAITIG simulations the monomers were kept in the interior of an 80 Å sphere by a quartic potential, modeling a 1.7 mg/mL aqueous solution; in the GAITIG simulations the monomers were placed in a periodically replicated 85 Å cubic box, modeling an 8.6 mg/mL solution. Both concentrations are within the range of experimental conditions in which the two peptides form fibers;[9] in general, larger peptides need lower concentrations for self-assembly, as done here. The higher GAITIG concentration was chosen to facilitate the observation of more complex sheets, involving all six monomers, in the relatively short duration of runs. All simulations were conducted with the program CHARMM, versions c35a1 and c35a2.[41]

Simulation Method. Both systems were simulated by the replica-exchange method.[31−36] For NSGAITIG, we conducted preliminary simulations in the temperature range 286−421 K. The average potential energies from these simulations were used in the iterative optimization of the replica temperatures as in refs 35 and 36 targeting exchange probabilities between adjacent (in temperature) replicas near ∼35−40%. In the final setup, we employed 18 replicas with temperatures 286, 293, 300, 307, 314, 321, 328, 333, 338, 343, 348, 353, 358, 363, 368, 373, and 380 K. The obtained exchange probabilities between adjacent replicas were 35 ± 8%; the replicas traveled the full $T_{min} - T_{max}$ interval 21 ± 10 times. In the GAITIG simulations, we employed 10 replicas, with temperatures 290, 300, 310, 320, 331, 342, 353, 364, 375, and 386 K. The exchange probabilities between adjacent replicas were 23 ± 2%, and the replicas traveled the full $T_{min} - T_{max}$ interval 14 ± 5 times. In both systems, replica exchanges were attempted at 10 ps intervals. The total simulation length at each temperature was 320 ns (NSGAITIG) and 400 ns (GAITIG).

In the early phase of the simulations (up to ∼80 ns), the individual peptides did not form extensive intermolecular interactions; subsequently, they were frequently involved in two- and three-stranded β-sheets (see Results). In what follows, we treated the simulation segment 0−80 ns as equilibration phase in both systems. Coordinates extracted from the last 240 ns (NSGAITIG) and 320 ns (GAITIG), at 10 ps intervals, were used in the analysis.

Secondary Structure Assignment. The secondary-structure content was assigned by the STRIDE algorithm.[42] Side-chain contacts were calculated with CHARMM subroutines;[41] two side chains were considered in contact if the distance between their geometric centers was less than 6 Å. Additional analysis of the conformational properties was performed with in-house FORTRAN programs.

Polar and Nematic Order Parameters P_1 and P_2. We assessed the extent of alignment and relative orientation of the individual peptides in the NSGAITIG trimer with the nematic order parameter P_2 and the polar order parameter P_1, defined in eq 1. These parameters are widely used in the structural characterization of anisotropic fluids such as liquid crystals[43−48] and have been employed successfully in simulation studies of peptide aggregation.[17]

$$P_1 = \frac{1}{N}\sum_{i=1}^{N}(\hat{z_i}, \hat{d})^2, \quad P_2 = \frac{1}{N}\sum_{i=1}^{N}\frac{3}{2}(\hat{z_i}, \hat{d})^2 - \frac{1}{2} \qquad (1)$$

In eq 1, N is the number of molecules in the simulation and $\hat{z}_i$ is a unit vector along a suitably defined molecular direction; $\hat{d}$ is a unit vector along a preferred direction of alignment, which emerges from the properties of the system.[49] In our calculations, $\hat{z}_i$ was defined along the lines Ala4(N)-Ile7(C). This choice was based on structural analysis of the conformations, which demonstrated that the moieties 4N-7C are the main constituents of the β-sheets observed in the simulations.

The parameter P_1 differentiates between parallel ($P_1 \approx 1$ for well-aligned, parallel strands) and antiparallel/mixed orientations ($P_1 \approx {}^1/_3$ for well-aligned strands). The parameter P_2 differentiates between ordered ($P_2 \approx 1$) and disordered conformations ($P_2 < \sqrt{[81/(40\pi N]}$), for a system of N peptides[50]); for NSGAITIG, $\sqrt{[81/(40\pi N])} = 0.46$ ($N = 3$). The parameters were computed with the WORDOM package.[51]

Using the values of P_1 and P_2 for three-stranded sheets, we constructed two-dimensional probabilities $P(P_1,P_2)$ and the corresponding free-energy surface

$$G(P_1, P_2) = -k_B T \ln[P(P_1, P_2)] \qquad (2)$$

Electrostatic Association Energies of β-Sheets. The formation electrostatic energies of β-sheets were computed by the relation

$$\Delta E_{assoc} = E_{k-strand} - \sum_{i=1}^{k} E_{strand\ i} \qquad (3)$$

where $E_{k-strand}$ was the energy of a particular β-sheet with k strands, and $E_{strand\ i}$ were the energies of the constituent strands i, when treated as isolated and immersed in water.

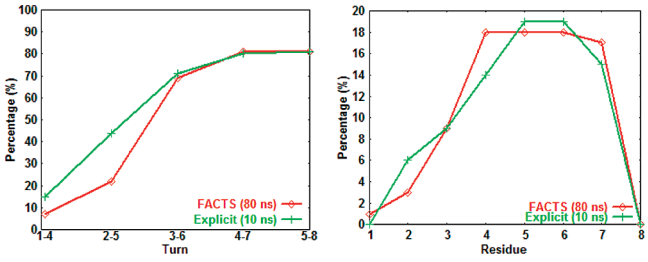

Figure 1. Probabilities of β-turn (left) and helix formation (right), computed from simulations of a single NSGAITIG peptide at 300 K. The red and green curves correspond, respectively, to explicit and implicit (all-atom FACTS) representations of the surrounding solvent.

Accuracy Check of the FACTS Implicit Solvent Model. To test the accuracy of the all-atom FACTS model used here,[37] we compared simulations of a single NSGAITIG peptide in implicit (FACTS) and explicit solvent. The FACTS simulations employed a replica-exchange method, with eight optimized temperatures spanning the range 283−432 K. The total simulation length was 80 ns.

The explicit-solvent runs employed a simulation system of a single peptide in a cubic, periodically replicated water box of 42 Å length. The peptide parameters were taken from the CHARMM22 all-atom force field[39] with the backbone CMAP grid correction.[52] The water was represented by a modified TIP3P model.[53,54] The electrostatic interactions were calculated without truncation by the particle-mesh Ewald method.[55] The temperature was maintained at 300 K by a Nose−Hoover thermostat[56] using a mass of 1000 kcal/ps^2 for the thermostat. The pressure was maintained at 1 atm by a Langevin piston[57] with a 500 amu mass, a 5 ps^{-1} collision frequency, and a bath temperature of 300 K. The classical equations of motion were integrated by the Leapfrog integrator, using a time step of 2 fs. Bond lengths to hydrogen atoms and the internal geometry of the water molecules were constrained with the SHAKE algorithm to standard values. We ran 10 different explicit-solvent simulations of 1.06 ns duration each at 300 K, starting from different initial conformations; the last 1 ns of each simulation was used in the analysis.

The secondary-structure content of the monomer in the explicit- and implicit-solvent simulations (300 K) is compared in Figure 1. The agreement between the two representations is excellent. The isolated NSGAITIG peptides have disordered N-terminal ends (residues Asn1 and Ser2) and the C-terminal moieties form often β-turns. A small fraction of helical conformations are also observed (Figure 1).

3. Results

In this section, we analyze the conformational properties of the two systems. We then quantify the interactions contributing to the stability of the observed conformations and interpret the differences among the two systems.

Conformational Analysis. ***NSGAITIG Trimer.*** The NSGAITIG sequence forms a turn-strand region in the native fold (the adenovirus fiber shaft), with the N-terminal residues N-S-G in the turn and the remaining residues in the β-strand.[27] The conformation of the isolated peptides NSGAITIG and GAITIG in solution is unknown, both at high dilution and in their amyloid fibrils. In the simulations of the NSGAITIG monomer, the N-terminal ends (residues 1−2) remain disordered and the C-terminal moiety folds mainly into β-turns (see Methods and Figure 1). In the NSGAITIG trimer simulations (as well as the GAITIG hexamer analyzed below), we observe the frequent formation of intermolecular β-sheets, in accordance with the amyloidogenic properties of the two peptides.[9]

The conformations adopted by the NSGAITIG trimer can be classified into six distinct states, depending on the number of present intermolecular β-sheets (0−1), the number of strands in a sheet (2−3), and the strand orientation [antiparallel (A), parallel (P), mixed (M)]. Using the notation PK (AK/MK) for a K-stranded, parallel (antiparallel/mixed) sheet, the five sheet-containing states are A2, P2, A3, P3, and M3. The left column of Figure 2 shows the time evolution of the probability (%) for these states at 300 K (upper row) and 368 K (lower row). In the early simulation phase at 300 K (up to ∼80 ns), the individual monomers form extensive intramolecular interactions, with the N-terminal residues Asn1 and Ser2 and the C-terminal moiety Gly3-Gly8 in β-turns or, less frequently, an α-helical conformation; this is in agreement with the conformations seen in the implicit- and explicit-solvent simulations of the individual monomers (Figure 1). In this early phase, the peptides also form two-stranded sheets, with populations which reach values of ∼20% (P2) and ∼15% (A2) at 80 ns. Later (after ∼80 ns), the peptides organize also in three-stranded β-sheets, composed of the C-terminal moieties (residues 3−8). The N-terminal residues Asn1-Ser2 remain disordered throughout the simulation (see below). This behavior is consistent with the native fold, i.e., the turn and strand motifs adopted, respectively, by the N- and C-terminal portions of the NSGAITIG sequence in the adenovirus fiber shaft.[27] Parallel arrangements dominate at 300 K, both in two- and three-stranded sheets.

Additional insights on the structural diversity of the observed three-stranded sheets can be obtained by analysis of their polar (P_1) and nematic (P_2) order parameters (defined in Methods) and their intermolecular main- and side-chain interactions. Figure 3 shows free-energy surfaces for the P3, A3, and M3 states at 300 K, generated from the corresponding two-dimensional probability densities $P(P_1,P_2)$ (eq 2). As explained in the Methods section, values of $P_2 > 0.46$ describe nonrandom alignment of the strands, with $P_2 \rightarrow 1$ for complete alignment; from the point of view of P_1, perfect orientation of the strands corresponds to $P_1 \rightarrow 1$ for parallel and $P_1 \rightarrow {}^1/_3$ for antiparallel/mixed sheets. Representative conformations are also shown. The structural and energetic properties of the three-stranded sheets are summarized in Table 1. Figure 4 shows probability-density maps of the main-chain hydrogen bonds and the side-chain contacts between the central (C) and edge (E) peptides of these sheets.

The parallel-sheet (P3) free-energy surface (Figure 3A) has one main basin ($P_1 = 0.7-1.0$, $P_2 = 0.4-1.0$), containing sheets with well-aligned strands and low polar and nonpolar energies (Table 1). The central and edge peptides of the sheets interact mainly in-register via their 5−7 moieties; these are also the dominant patterns in the corresponding hydrogen-bonding and side-chain contact density maps (Figure 4A,D). The charged N-terminal ends are solvent-exposed, disordered, and well separated (the distance between the terminal N atoms is 14 ± 4 Å). Presumably, the screened electrostatic repulsion of the N-termini and the good alignment of the C-terminal 5−7 moieties contribute to the low polar and nonpolar energies. A second, less populated basin ($P_1 = 0.3-0.7$, $P_2 = 0.3-0.6$) has sheets, which maintain the in-register interactions 5−7C/5−7E but are more disordered in the region 1−4 and have higher nonpolar energies (Table 1).

The A3 free-energy surface (Figure 3B) has two main basins. The first ($P_1 = 0.2-0.4$, $P_2 = 0.4-0.9$) has well-aligned sheets

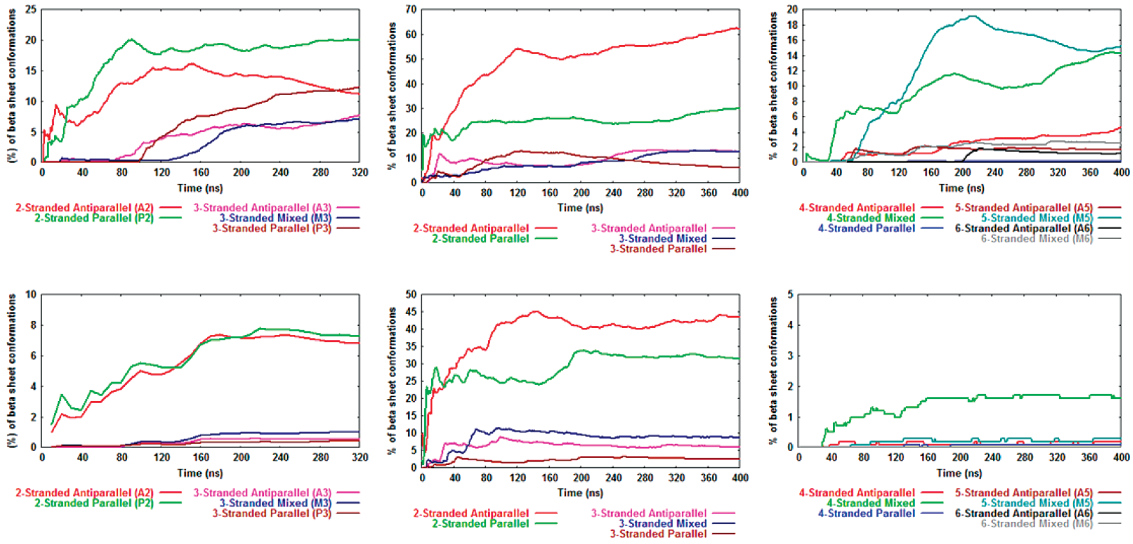

Figure 2. Running averages of the fraction (%) of conformations with intermolecular β-sheets in the NSGAITIG/GAITIG simulations. Left column: NSGAITIG trimer. Middle and right columns: GAITIG hexamer. The upper row corresponds to the 300 K simulations for both systems; the lower row corresponds to 368 K (NSGAITIG) and 384 K (GAITIG).

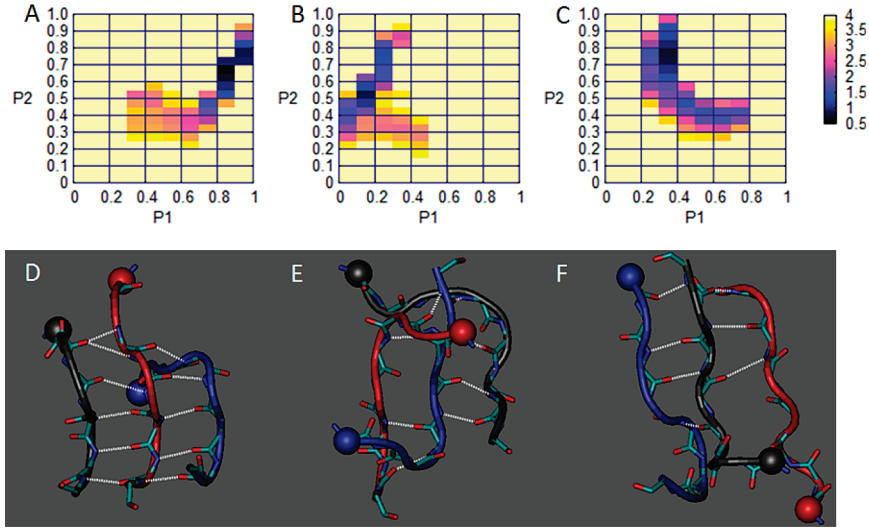

Figure 3. (Upper row) Two-dimensional free energy surfaces for the NSGAITIG three-stranded sheets at 300 K, constructed by the two-dimensional probability of the order parameters P_1 and P_2 (discussed in Methods): (A) parallel, (B) antiparallel, and (C) mixed sheets. (Bottom row) Representative conformations of the most important basins in the above surfaces: (D) parallel sheet ($P_1 = 0.96$, $P_2 = 0.88$); (E) antiparallel sheet ($P_1 = 0.33$ $P_2 = 0.95$); (F) mixed sheet ($P_1 = 0.31$, $P_2 = 0.90$). Hydrogen bonds are shown in white dashed lines. The N-terminal Cα atoms are shown in vdW representation; side chains are omitted.

with, mainly, the off-register hydrogen-bonding patterns 4−7C/6−3E, 5−7C/7−5E (Figure 4B). The second basin [(P_1 = 0.0−0.1, P_2 = 0.2−0.55) ∪ (P_1 = 0.1−0.2, P_2 = 0.4−0.7)] has less aligned sheets, with shorter hydrogen-bonding patterns (4−5C/6−5E, 3−5C/6−4E, 4−5C/7−6E). A small fraction of conformations (0.5%) are in the region (P_1 = 0.1−0.5, P_2 = 0.2−0.4). These sheets have unaligned strands, forming antiparallel β-bridges (2C/7E, 4C/7E). Often, one of the edge strands turns and forms an additional parallel β-bridge with the central strand. As a result, the bonded energies of these conformations are higher by ∼2 kcal/mol, even though their total nonbonded energies are comparable with the other two basins (see Table 1).

The free-energy surface of mixed sheets (Figure 3C) has two basins in the regions (P_1 = 0.2−0.4, P_2 = 0.6−1.0) and (P_1 = 0.2−0.8, P_2 = 0.3−0.6). The first basin contains somewhat more aligned sheets. The nonbonded energies of the mixed sheets are higher with respect to the parallel sheets, mainly due to the nonpolar components.

Representative conformations of the most important basins in the parallel, antiparallel, and mixed β-sheet surfaces of Figure 3A−C are shown, respectively, in Figure 3, D, E, and F.

Table 2 lists the important main-chain/side-chain interactions, observed in the 300 K simulations. The side-chain of Thr6 forms extensive hydrogen-bonding interactions, with the main-chain moieties of residues Ser2, Gly3, and Ile5 (parallel sheets), and Ser2, Ala4 (antiparallel sheets). Thus, it is likely that Thr6 plays an important role in the formation and/or stabilization of the NSGAITIG amyloid nanostructures. An additional frequent interaction in antiparallel sheets is between the side chain of Ser2 and the main chain of Ile7. Despite the side-chain interactions mentioned above, the main chain of Ser2 and also Asn1 rarely participate in the β-sheets observed in the simulations (Figure 4A−C). This suggests that they are as not important in the amyloid self-assembly of NSGAITIG as the C-terminal moiety Gly3-Gly7, in accord with earlier experiments, which demonstrated that the hexapeptide GAITIG also forms amyloid fibers.[9]

TABLE 1: Properties of the P1−P2 Free-Energy Surfaces (Figure 3), Describing NSGAITIG Three-Stranded β-Sheets at 300 K

basin	probability[a] (%)	(P_1,P_2)[b] range	energies (kcal/mol)[d] polar	nonpolar	total[e]
		P3[c]			
1	14.5	(0.7–1.0, 0.4–1.0)	–463.9 (8.7)	–23.1 (8.4)	–487.0 (10.4)
2	1.0	(0.3–0.7, 0.3–0.6)	–464.8 (8.6)	–16.9 (9.2)	–481.7 (10.6)
		A3[c]			
1	3.0	(0.2–0.4, 0.4–0.9)	–458.7 (8.2)	–18.8 (7.6)	–477.5 (9.7)
2	6.5	(0.0–0.1, 0.2–0.55)∪ (0.1–0.2, 0.4–0.7)	–456.7 (8.9)	–22.0 (7.3)	–478.9 (10.1)
3	0.5	(0.1–0.5, 0.2–0.4)	–458.6 (9.1)	–18.3 (7.3)	–476.9 (10.9)
		M3[c]			
1	5.2	(0.2–0.4, 0.6–1.0)	–463.4 (8.6)	–18.0 (7.7)	–481.4 (9.7)
2	3.9	(0.2–0.8, 0.3–0.6)	–463.8 (9.2)	–17.0 (7.7)	–480.9 (9.9)

[a] Fraction (%) of conformations in the corresponding basin (out of 24 000 snapshots at 1 ps intervals, spanning the simulation segment 8−32 ns). [b] The polar (P_1) and nematic (P_2) order parameters are defined in the Methods section. Ranges of values pertaining to the corresponding basin are listed. [c] P3, M3, and A3 denote parallel, antiparallel, and mixed three-stranded β-sheets. [d] Average values and standard deviations (in parentheses) over conformations in the corresponding basins are listed. [e] Sum of polar and nonpolar energies.

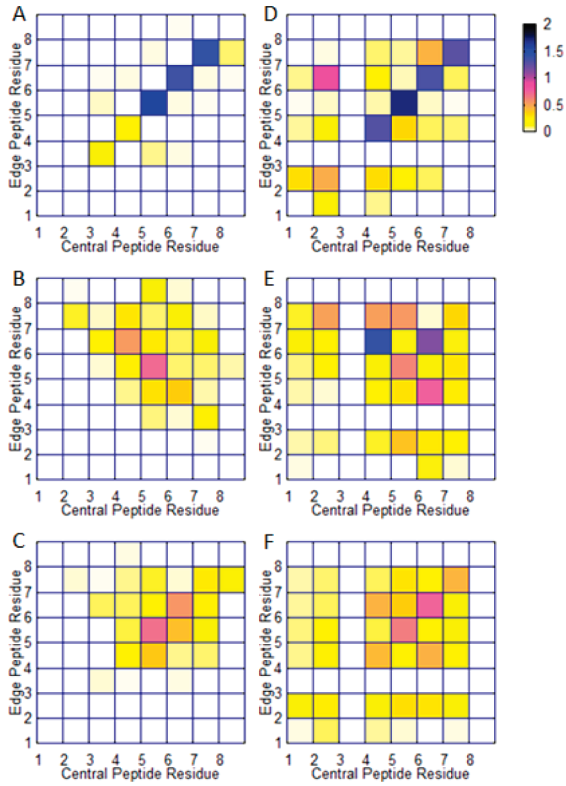

Figure 4. Probability density maps of main-chain hydrogen bonds (left column) and side-chain contacts (right column) between the central and edge peptides of three-stranded NSGAITIG β-sheets at 300 K. The rows from top to bottom correspond, respectively, to parallel, antiparallel, and mixed sheets.

The intermolecular side-chain contacts of parallel sheets (Figure 4D) are well correlated with the main-chain hydrogen-bonding patterns. In antiparallel sheets (Figure 4E), this correlation is not as strong. This is partly due to the fact that the antiparallel sheets form a larger variety of hydrogen-bonding patterns (Figure 4B). An important off-register contact in antiparallel sheets corresponds to the pair Thr6-Thr6; visual inspection of the trajectories showed that the hydrophobic moieties of the two threonine side chains tend to pack against each other. Other frequent side-chain contacts (mainly in antiparallel and mixed conformations) are between the N-terminal residues (Asn1, Ser2) and the 4−7 moiety.

TABLE 2: Important Intermolecular Main-Chain/Side-Chain Hydrogen Bonds, Observed in Three-Stranded β-Sheets of the NSGAITIG System at 300 K

sheet type[a]	main chain	side chain	occupancy
P	Ile5(O)	Thr6(HG1)	0.88
	Ser2(O)	Thr6(HG1)	0.50
	Gly3(HN)	Thr6(OG1)	0.34
A	Ser2(O)	Thr6(HG1)	0.46
	Ala4(HN)	Thr6(OG1)	0.36
	Ile7(O)	Ser2(HG1)	0.30
M	Ile5(O)	Thr6(HG1)	0.30
	Ile7(O)	Ser2(HG1)	0.27
	Ala4(HN)	Thr6(OG1)	0.25

[a] P, M, and A denote, respectively, parallel, antiparallel, and mixed β-sheets.

GAITIG Hexamer. In the case of the GAITIG hexamer, each conformation may contain up to three parallel and/or antiparallel sheets with sizes between 2 and 6 strands, and up to two mixed sheets with sizes between 3 and 6 strands. An exact enumeration of states is given below. Here we investigate the appearance of β-sheet elements.

The middle and right columns of Figure 2 plot the time evolution of the fraction (%) of conformations with (at least one) intermolecular β-sheet elements at 300 K (upper row) and 364 K (lower row). Some conformations contribute to more than one curve. For example, one conformation which contains one two-stranded antiparallel sheet and one three-stranded parallel sheet contributes to both curves "three-stranded antiparallel sheets", and "two-stranded parallel sheets".

In the first ∼40−80 ns, the peptides start to organize into two- and three-stranded sheets. Progressively, sheets with four to six strands are also observed. The populations of these sheets are small (especially at the higher temperature) and do not entirely converge in the time course of the simulation. Interestingly, the antiparallel orientation is thermodynamically preferred with respect to the parallel, in contrast to the behavior of the NSGAITIG solution. The difference between the two systems is interpreted below with energetic calculations.

A more detailed classification of the hexamer conformations takes into account the exact number of simultaneously present parallel, antiparallel, and mixed intermolecular β-sheets and the number of strands in each sheet. The 38 resulting states are included as labels along the horizontal axis of Figure 5. We use the same notation as for NSGAITIG, above; i.e., PK (AK/MK) denotes the existence of a parallel (antiparallel/mixed),

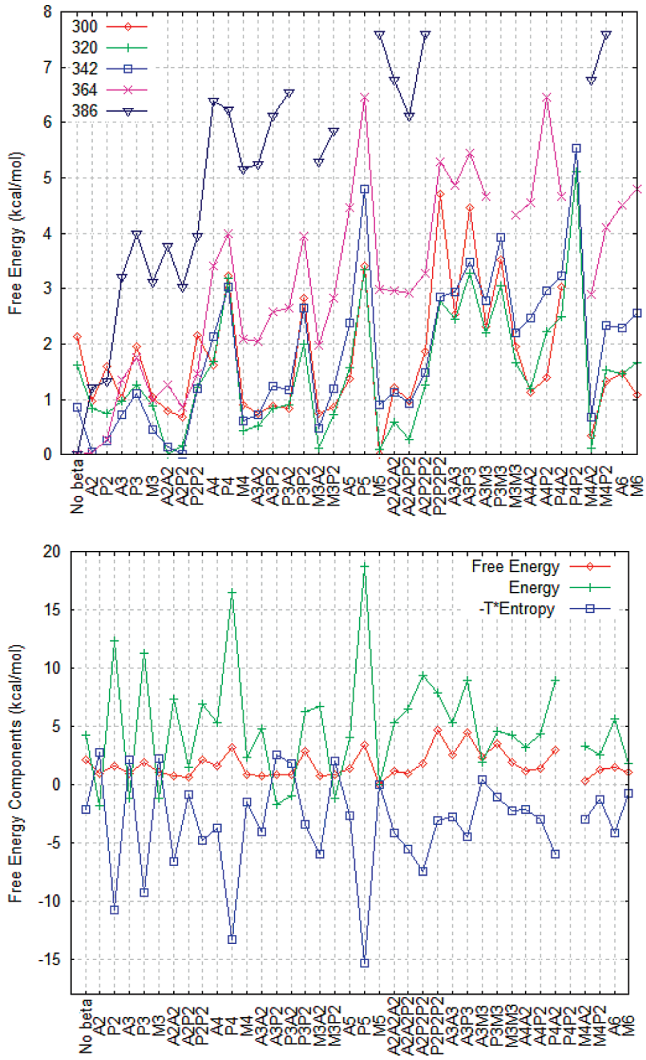

Figure 5. (Upper plot) Free energy profiles of the 38 possible conformational states for the GAITIG hexamer. The states are shown in the horizontal axis; PK(AK/MK) denote a parallel (antiparallel/mixed) β-sheet with k strands. For example, "A2P2" is a state with one antiparallel and one parallel two-stranded sheet, and the remaining two monomers not engaged in β-sheet interactions. Each profile is plotted relative to the free energy of the most frequent state (at the same temperature). (Lower plot) Decomposition of the free energy profile of the GAITIG hexamer at 300 K into energetic and entropic components (see text). The profiles are plotted relative to the value for the most probable state (M5).

K-stranded sheet in the hexamer. With this notation, P2A2A2 denotes a state with one parallel, two-stranded sheet and two antiparallel, two-stranded sheets (see also the legend of Figure 5). Free energy profiles of these states are shown in the top plot of Figure 5. In the profiles, the states are arranged (from left to right) in order of increasing complexity. For example, the states at the left end of the profiles have no sheets (state "no beta"), or one sheet (states A2-M3); at the right end (states A2A2A2-M6), all monomers participate in β-sheets.

States with parallel sheets (P5, P4, P4P2, P3P2) have low relative probability at all temperatures. At lower temperatures (300−342 K), the most populated states contain mixed and/or antiparallel sheets (states M5, M4A2, M3A2, A2A2, A2P2). At higher temperatures (364−386 K), random conformations become dominant, as expected. Examples of the most complex β-sheet structures (A5, M5, A6, M6), observed at 300 K, are shown in Figure 6.

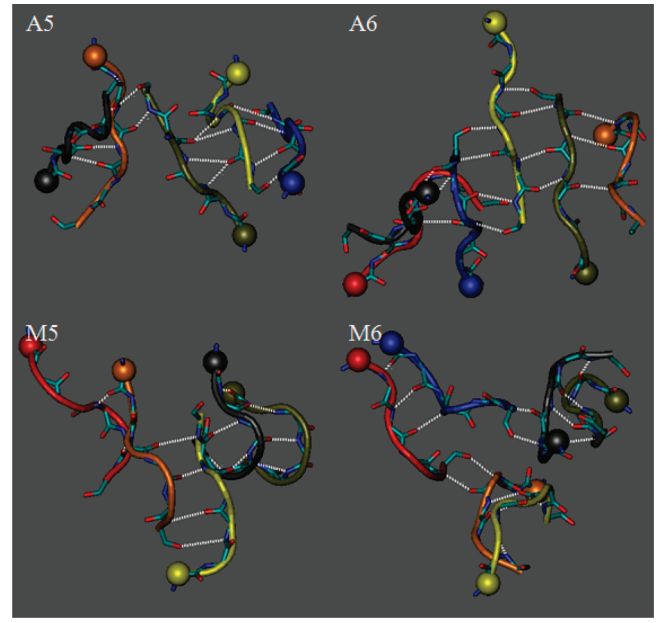

Figure 6. Representative 5- and 6-stranded antiparallel (A5,A6) and mixed (M5,M6) β-sheets, observed in the 300 K GAITIG hexamer simulations. Hydrogen bonds are shown in white dashed lines; the N-terminal Cα atoms are shown in vdW representation. The peptide not participating in the sheets (A5 and M5 plots) and all side chains are omitted.

The lower plot of Figure 5 includes a decomposition of the free-energy profile at 300 K into "energetic" and "entropic" components. To compute the energy profile, we averaged the total energy of the hexamer over the conformations of each individual state (due to the implicit-solvent model, the energy profile includes an entropic contribution). The entropy profile ($-T*S$) is the difference between the free-energy and energy profiles. In general, states with high free energy (low probability) are also associated with high energies.

Conformations with one antiparallel sheet (A2, A3, ...) have lower energies compared to conformations with one parallel sheet of the same size (P2, P3, ...), due to both polar and nonpolar interactions. Interestingly, states with extended mixed sheets can have lower energies than states with antiparallel sheets of the same size (e.g., M4 vs A4, M5 vs A5). This is mainly to a lower GB interaction energy component in these mixed-sheets, presumably arising from the higher polarization of the solvent due to approach of similar-sign charges. The energetic stabilization of antiparallel sheets with respect to parallel sheets does not always hold in conformations with several coexisting sheets (e.g., A2A2 and A3A2 have higher energies, respectively, than A2P2 and A3P2). This holds due to a competition between polar and nonpolar interactions in the entire aggregates.

Figure 7 shows density maps of intermolecular interactions, characterizing the GAITIG β-sheets at 300 K; antiparallel and parallel sheets are analyzed in the left and right column, respectively. Plots 7A−D and 7F−H show maps of main-chain hydrogen bonds in 2- to 6-stranded sheets (patterns for the less-frequent 5- and 6-stranded antiparallel sheets are combined in plot 7D). Both in antiparallel and parallel sheets, the principal hydrogen-bonding interactions between adjacent strands involve the main chains of moieties I3−I5.

The GAITIG hexapeptide contains only one side chain with hydrogen-bonding capacity (Thr4). This side-chain forms infrequent intermolecular interactions with the main-chain

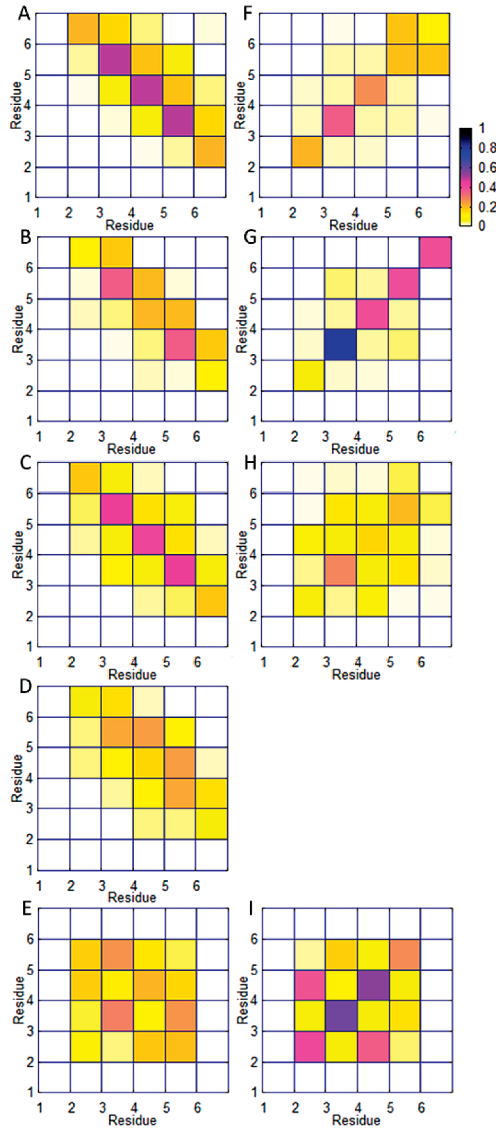

Figure 7. Density maps of interactions observed in the GAITIG β-sheets at 300 K. The left and right columns correspond, respectively, to antiparallel and parallel sheets. First four rows (top to bottom): Maps of main-chain hydrogen bonds in two- to six-stranded sheets (the fourth-row map shows the combined probability of five- and six-stranded antiparallel sheets). Last row: side-chain contacts in β-sheets of any size.

carbonyl of Ala2 (in parallel sheets) and the amide group of Thr4 (in antiparallel sheets).

The bottom row of Figure 7 contains density maps of side-chain contacts for sheets of any size. In antiparallel sheets (7E), the most important contacts correspond to the pairs Ile3-Ile5, Thr4-Thr4, and Ile3-Ile3; the first two correlate with the predominant hydrogen-bonding pattern. In parallel sheets (7I), the most important contacts are in-register (Ala2-Ala2, Ile3-Ile3, Thr4-Thr4, Ile5-Ile5). An additional, important off-register contact corresponds to Ala2-Thr4. The side-chain to side-chain contact probabilities are higher overall in parallel sheets.

Energetic Analysis of the β-Sheets at 300 K. The present simulations suggest that the NSGAITIG octapeptide has a higher propensity for parallel, compared to antiparallel or mixed β-sheets, at least in the simulated trimer. To interpret this preference, we performed an energetic analysis of the three-stranded sheets at 300 K. The total energies are listed in Table 3, along with a decomposition into bonded and nonbonded components. The intermolecular interaction Coulomb energies (eq 3) are included in Table 4.

TABLE 3: Average Total Energies of Selected β-Sheet Conformations at 300 K (in kcal/mol)

ST[a]	total	bonded	nonbonded	nonpolar	polar	GB	Coulomb
NSGAITIG 3-Stranded Sheets							
P	–168	318	–486	–22	–464	–358	–105
A	–160	319	–479	–21	–458	–359	–100
M	–162	320	–482	–18	–464	–360	–104
GAITIG 3-Stranded Sheets							
P	–1090	480	–1570	–57	–1513	–1602	89
A	–1126	480	–1606	–57	–1549	–1613	64
M	–1122	480	–1602	–57	–1545	–1615	70

[a] P, A, and M denote parallel, antiparallel, and mixed sheets. The nonpolar energy is the sum of the van der Waals energy and a component proportional to the total surface area. The polar energy is the sum of Coulomb and GB(FACTS) energies.

TABLE 4: Average Intermolecular Coulomb Energies of Selected β-Sheet Conformations at 300 K (in kcal/mol)

ST[a]	total	backbone–backbone	backbone–side chain	side chain–side chain
NSGAITIG 3-Stranded Sheets				
P	–86	–52	–55	22
A	–63	–38	–45	18
M	–65	–41	–43	21
GAITIG 3-Stranded Sheets				
P	–19	–30	+9	2
A	–53	–46	–10	3
M	–47	–42	–8	3

[a] P, A, and M denote parallel, antiparallel, and mixed sheets.

Parallel sheets are associated with the lowest average total energy, in line with their higher propensity. They are stabilized with respect to antiparallel sheets, mainly due to a lower total Coulomb energy (last column of Table 3). This arises from stronger intermolecular Coulomb interactions among the main-chain and side-chain moieties of individual strands (second and third column of Table 4), in line with the stronger intermolecular main chain−main chain and main chain−side chain hydrogen bonds of parallel β-sheets (Figure 4A and Table 2).

In the case of GAITIG, conformational states with parallel (antiparallel) sheets are associated with low (high) probabilities and high (low) energies, as shown above. The energetic profile of Figure 6 displays the total energies of the hexamers; these energies depend not only on the individual sheets but also on the surrounding background (the peptides not participating in the sheets). To understand better the energetic differences between parallel and antiparallel GAITIG sheets, in Table 3 we compare the energies of the three-stranded sheets. In the reported values, the interactions involving the three peptides not participating in the sheets are ignored.

Antiparallel sheets are more stable energetically by 36 kcal/mol with respect to parallel sheets. This is due to the Coulombic component (last column of Table 3). Table 4 lists the intermolecular Coulombic components among the constituent strands. The Coulombic interactions among different strands are significantly higher in parallel sheets (−19 kcal/mol), compared to antiparallel (−53 kcal/mol). This is mainly due to backbone interactions, and specifically due to the repulsion among the charged N-terminal ends (respectively, 19.0 and 0.5 kcal/mol, in parallel and antiparallel sheets). In the longer NSGAITIG octapeptide, this repulsion is reduced (11.5 and 2.3 kcal/mol in the three-stranded sheets) and the total energy is more negative in parallel sheets. As explained above, the N-terminal ends of

the NSGAITIG peptides remain solvent-exposed, disordered and relatively far from the β-sheet core moiety.

4. Discussion and Conclusions

In the present work, we have investigated the conformational properties of the amyloidogenic octapeptide NH_3-NSGAITIG-NH_2 and the related hexapeptide NH_3-GAITIG-NH_2[9] by molecular dynamics simulations. In the NSGAITIG simulations, the C-terminal moieties (Ala4-Ile7) demonstrated a propensity for intermolecular β-sheets, in accord with the amyloidogenic ability of the hexapeptide NH_3-GAITIG-NH_2 demonstrated in ref 9. At the same time, the N-terminal residues Asn1 and Ser2 of NSGAITIG are not engaged in the sheets. This is consistent with the turn and strand motifs adopted, respectively, by the N- and C-terminal portions of the NSGAITIG sequence in the adenovirus fiber shaft.[27] Presumably, the N-terminal residues are not engaged in the cross-beta core within the fibrils, and therefore they should be exposed at the exterior of the fibril and accessible. These positions are therefore suitable candidates for rationally modifying this amyloid-forming building block to enable it for specific binding of ligands and technological applications. One basic requirement is that the modifications should not affect the capability for self-assembly; hence they should be introduced at positions not engaged in the amyloid-forming core. Based on insight provided by the simulations, cysteine residues were recently substituted at positions 1 and 2; the newly designed peptides formed amyloid fibrils capable of binding to silver, gold, and platinum nanoparticles, confirming the accessibility of the residues at these positions.[38]

The charged N-terminal ends (+1) of the peptides do not destabilize the parallel orientation in the NSGAITIG trimers (the average Coulomb interaction energies among the N-terminal main-chain atoms of Asn1 are, respectively, 11.5, 4.0, and 2.3 kcal/mol, in the parallel, mixed and antiparallel three-stranded sheets of the 300 K simulations). This is because the N-terminal ends remain well separated and well exposed to the solvent; eg., as discussed above, the average distance between the N-terminal nitrogen atoms is 14 ± 4 Å in the parallel sheets of the most populated basin of the P1−P2 surface (Figure 3A). In comparison, the corresponding Coulomb interaction energies among the C-terminal main-chain moieties (residues 4−8) are −46.3, −28.4, and −20.7 kcal/mol, respectively, in three-stranded parallel, mixed, and antiparallel sheets. The lower Coulomb interaction energies of parallel sheets (Table 4) are mainly due to stronger main-chain/main-chain hydrogen bonds and main-chain/side-chain interactions (Figure 4 and Table 2). The parallel sheets may be further stabilized by interactions among in-register side chains.[21,58−63] Indeed, the C-terminal moiety of NSGAITIG has hydrophobic residues, which constitute the core of the observed β-sheets and form extensive side-chain interactions (Figure 4). Nevertheless, the populations of three-stranded antiparallel and mixed sheets are also high (~2/3 of the parallel-sheet population at 300 K). Given the fact that the simulated system is small (three peptides), the parallel orientation may not be the dominant one in the actual NSGAITIG fibrillar assemblies. A combination of arrangements is also possible, e.g., parallel strands within each β-sheet, and adjacent sheets in antiparallel orientation (e.g., as in Figure 1B of ref 3) is also possible.

In the GAITIG sheets, the average distance among the N-terminal ends is smaller (8.4 ± 4.0 Å in three-stranded parallel sheets), compared to the corresponding distance in the longer NSGAITIG sheets. As a result, the Coulomb interactions among the N-terminal ends can destabilize the parallel orientation, with respect to the antiparallel (Table 3). The propensity for the antiparallel orientation is increased compared to the parallel in the entire temperature range.

By utilizing an all-atom representation for the peptides, the present study has provided detailed information (e.g., hydrogen-bonding interactions, side-chain contacts) on the behavior of the aggregates formed in the initial self-assembly process and on the likely molecular organization of the NSGAITIG and GAITIG amyloid fibers. Even when combined with an implicit modeling of solvent effects, as done here, atomic-resolution peptide models are still limited to small sizes and time scales and are better suited to study the early stages of aggregate formation. Lower resolution (coarse-grained) protein models can prove very useful in studying the entire aggregation process, from oligomeric to fibrillar species.[16,19,23,24]

In summary, in the present work we have performed a computational investigation of the self-assembly of two amyloidogenic sequences from the adenovirus fiber shaft. Our findings suggest that the amyloidogenic propensity of the NSGAITIG sequence lies mainly in the hydrophobic moiety AITI. The N-terminal residues Asn1 and Ser2 of NSGAITIG are thus likely to be exposed at the exterior of the fibril and accessible, in accord with the amyloidogenic capacity of the smaller sequence (GAITIG).[9] These positions are therefore suitable candidates for rational modifications of this amyloid-forming building block, aiming at the fabrication of advanced technological biomaterials. Indeed, we have recently substituted cysteine residues at positions 1 and 2; the newly designed peptides form amyloid fibrils which bind to silver, gold, and platinum nanoparticles. Such metal-binding peptides with self-assembling properties may have a potential use as conducting nanowires, with applications in nanocircuitry.[38]

Acknowledgment. G.A. and Ph.T. thank Prof. Amedeo Caflisch for helpful comments. We thank the anonymous referees for helpful comments. The work was funded by a grant from the A.G. Leventis Foundation (to G.A. and Ph.T). E.K. and A.M. acknowledge support from the European Union (STREP NMP4-CT-2006-033256, "BeNatural". All simulations were performed on Linux clusters of the Biophysics group at the University of Cyprus.

References and Notes

(1) Chiti, F.; Dobson, C. M. *Annu. Rev. Biochem.* **2006**, *75*, 333–366.
(2) Bemporad, F.; Galloni, G.; Campioni, S.; Plakoutsi, G.; Taddei, N.; Chiti, F. *Acc. Chem. Res.* **2006**, *39*, 620–627.
(3) Nelson, R.; Eisenberg, D. *Adv. Protein Chem.* **2006**, *73*, 235–282.
(4) Harrison, R. S.; Sharpe, P. C.; Singh, Y.; Fairlie, D. P. *Rev. Physiol. Biochem. Pharmacol.* **2007**, *159*, 1–77.
(5) Gazit, E. *Chem. Soc. Rev.* **2007**, *36*, 1263–1269.
(6) Zhao, X. J.; Zhang, S. G. *Macromol. Biosci.* **2007**, *7*, 13–22.
(7) Colombo, G.; Soto, P.; Gazit, E. *Trends Biotechnol.* **2007**, *25*, 211–218.
(8) Chockalingam, K.; Blenner, M.; Banta, S. *Protein Eng., Des. Sel.* **2007**, *20*, 155–161.
(9) Papanikolopoulou, K.; Schoehn, G.; Forge, V.; Forsyth, V. T.; Riekel, C.; Hernandez, J. F.; Ruigrok, R. W. H.; Mitraki, A. *J. Biol. Chem.* **2005**, *280*, 2481–2490.
(10) Sawaya, M. R.; Sambashivan, S.; Nelson, R.; Ivanova, M. I.; Sievers, S. A.; Apostol, M. I.; Thompson, M. J.; Balbirnie, M.; Wiltzius, J. J. W.; McFarlane, H. T.; Madsen, A. O.; Riekel, C.; Eisenberg, D. *Nature* **2007**, *447*, 453–457.
(11) Knowles, T. P.; Fitzpatrick, A. W.; Meehan, S.; Mott, H. R.; Vendruscolo, M.; Dobson, C. M.; Welland, M. E. *Science* **2007**, *318*, 1900–1903.
(12) Mesquida, P.; Riener, C. K.; MacPhee, C. E.; McKendry, R. A. *J. Mater. Sci. Mater. Med.* **2007**, *18*, 1325–1331.
(13) Zanuy, D.; Porat, Y.; Gazit, E.; Nussinov, R. *Structure* **2004**, *12*, 439–455.

(14) Mousseau, N.; Derreumaux, P. *Acc. Chem. Res.* **2005**, *38*, 885–891.
(15) Ma, B. Y.; Nussinov, R. *Curr. Op. Chem. Biol.* **2006**, *10*, 445–452.
(16) Hall, C. K.; Wagoner, V. A. *Methods Enzymol.* **2007**, *412*, 338–365.
(17) Cecchini, M.; Rao, F.; Seeber, M.; Caflisch, A. *J. Chem. Phys.* **2004**, *121*, 10748–10756.
(18) Paci, E.; Gsponer, J.; Salvatella, X.; Vendruscolo, M. *J. Mol. Biol.* **2004**, *340*, 555–569.
(19) Pellarin, R.; Guarnera, E.; Caflisch, A. *J. Mol. Biol.* **2007**, *374*, 917–924.
(20) Nguyen, P. H.; Li, M. S.; Stock, G.; Straub, J. E.; Thirumalai, D. *Proc. Natl. Acad. Sci. U.S.A.* **2007**, *104*, 111.
(21) Hills, R. D.; Brooks, C. L., III. *J. Mol. Biol.* **2007**, *368*, 894–901.
(22) Tarus, B.; Straub, J. E.; Thirumalai, D. *J. Mol. Biol.* **2008**, *379*, 815–829.
(23) Song, W.; Wei, G.; Mousseau, N.; Derreumaux, P. *J. Phys. Chem. B* **2008**, *112*, 4410–4418.
(24) Bellesia, G.; Shea, J. E. *J. Chem. Phys.* **2009**, *130*, 145103.
(25) Tamamis, P.; Adler-Abramovich, L.; Reches, M.; Marshall, K.; Sikorski, P.; Serpell, L.; Gazit, E.; Archontis, G. *Biophys. J.* **2009**, *96*, 5020–5029.
(26) Mitraki, A.; Papanikolopoulou, K.; van Raaij, M. J. *Adv. Protein Chem.* **2006**, *73*, 97–124.
(27) van Raaj, M. J.; Mitraki, A.; Lavigne, G.; Cusack, S. *Nature* **1999**, *401*, 935–938.
(28) Hong, J.; Engler, J. A. *J. Virol.* **1996**, *70*, 7071–7078.
(29) Papanikolopoulou, K.; Teixeria, S.; Belrhali, H.; Forsyth, V. T.; Mitraki, A.; van Raaij, M. J. *J. Mol. Biol.* **2004**, *342*, 219–227.
(30) Luckey, M.; Hernandez, J.-F.; Arlaud, G.; Forsyth, V. T.; Ruigrok, R. W. H.; Mitraki, A. *FEBS Lett.* **2000**, *468*, 23–27.
(31) Swendsen, R.; Wang, J. *Phys. Rev. Lett.* **1986**, *57*, 2607–2609.
(32) Hansmann, U. *Chem. Phys. Lett.* **1997**, *281*, 140–150.
(33) Sugita, Y.; Okamoto, Y. *Chem. Phys. Lett.* **1999**, *314*, 141–151.
(34) Nymeyer, H.; Gnanakaran, S.; Garcia, A. E. *Methods Enzymol.* **2004**, *30*, 119–149.
(35) Hukushima, K.; Nemoto, K. *J. Phys. Soc. Jpn.* **1996**, *65*, 1604–1608.
(36) Sanbonmatsu, K. Y.; Garcia, A. E. *Proteins* **2002**, *46*, 225–234.
(37) Haberthür, U.; Caflisch, A. *J. Comput. Chem.* **2008**, *29*, 701–715.
(38) Kasotakis, E.; Mossou, E.; Adler-Abramovich, L.; Mitchell, E. P.; Forsyth, V. T.; Gazit, E.; Mitraki, A. *Biopolymers* **2009**, *92*, 164–172.
(39) MacKerrell, A. D. Jr.; Bashford, D.; Bellott, M.; Dunbrack, R. L.; Evanseck, J. D.; Field, M. J.; Fischer, S.; Gao, J.; Guo, H.; Ha, S.; Joseph-McCarthy, D.; Kuchnir, L.; Kuczera, K.; Lau, F. K. T.; Mattos, C.; Michnick, S.; Ngo, T.; Nguyen, D. T.; Prodhom, B.; Reiher, W. E. III.; Roux, B.; Schlenkrich, M.; Smith, J. C.; Stote, R.; Straub, J.; Watanabe, M.; Wiorkewicz-Kuczera, J.; Yin, D.; Karplus, M. *J. Phys. Chem. B* **1998**, *102*, 3586–3616.
(40) Ryckaert, J. P.; Ciccotti, G.; Berendsen, H. J. C. *J. Comput. Phys.* **1997**, *23*, 327–341.
(41) Brooks, B. R.; Brooks, C. L. III; Mackerell, A. D. Jr.; Nilsson, L.; Petrella, R. J.; Roux, B.; Won, Y.; Archontis, G.; Bartels, C.; Boresch, S.; Caflisch, A.; Caves, L.; Cui, Q.; Dinner, A. R.; Feig, M.; Fischer, S.; Gao, J.; Hodoscek, M.; Im, W.; Kuczera, K.; Lazaridis, T.; Ma, J.; Ovchinnikov, V.; Paci, E.; Pastor, R. W.; Post, C. B.; Pu, J. Z.; Schaefer, M.; Tidor, B.; Venable, R. M.; Woodcock, H. L.; Wu, X.; Yang, W.; York, D. M.; Karplus, M. *J. Comput. Chem.* **2009**, *30*, 1545–1614.
(42) Frishman, D.; Argos, P. *Proteins* **1995**, *23*, 566–579.
(43) Chandrasekhar, S. *Liquid Crystals*; Cambridge University Press: Cambridge, England, 1992.
(44) de Gennes, P. G. Prost, J. *The Physics of Liquid Crystals*, 2nd ed.; Oxford University Press: Oxford, UK, 1993.
(45) Zannoni, C. *J. Mater. Chem.* **2001**, *11*, 2637–2646.
(46) Berardi, R.; Muccioli, L.; Zannoni, C. *ChemPhysChem.* **2004**, *5*, 104–111.
(47) Rose, M. E. *Elementary Theory of Angular Momentum*; Wiley: New York, 1957.
(48) Zannoni, C. *The Molecular Physics of Liquid Crystals*; Academic: London, 1979; Chapter 3.
(49) Allen, M. P. Tildesley. D. J. *Computer Simulation of Liquids*; Oxford Science: Oxford, UK, 1987.
(50) Doerr, T. P.; Heman, D.; Mathur, H.; Taylor, P. L. *Europhys. Lett.* **2002**, *59*, 398–402.
(51) Seeber, M.; Cecchini, M.; Rao, F.; Settanni, G.; Caflisch, A. *Bioinformatics* **2007**, *23*, 2625–2627.
(52) Mackerell, A. D. Jr.; Feig, M.; Brooks, C. L., III. *J. Comput. Chem.* **2004**, *25*, 1400–1415.
(53) Jorgensen, W. L.; Chandrasekhar, J.; Madura, J. D.; Impey, R. W.; Klein, M. L. *J. Chem. Phys.* **1983**, *79*, 926–935.
(54) Neria, E.; Fischer, S.; Karplus, M. J. *Chem. Phys.* **1996**, *105*, 1902–1921.
(55) Darden, T.; York, D.; Pedersen, L. *J. Chem. Phys.* **1993**, *98*, 10089–10092.
(56) Nose, S. *J. Chem. Phys.* **1984**, *81*, 511–519.
(57) Feller, S.; Zhang, Y.; Pastor, R. W.; Brooks, B. *J. Chem. Phys.* **1995**, *103*, 4613–4621.
(58) Tartaglia, G.; Cavalli, G. A.; Pellarin, R.; Caflisch, A. *Protein Sci.* **2005**, *14*, 2723–2734.
(59) Cecchini, M.; Curcio, R.; Pappalardo, M.; Melki, R.; Caflisch, A. *J. Mol. Biol.* **2006**, *357*, 1306–1321.
(60) Kajava, A. V.; Baxa, U.; Wickner, R. B.; Steven, A. C. *Proc. Natl. Acad. Sci. U.S.A.* **2004**, *101*, 7885–7890.
(61) Kajava, A. V.; Aebi, U.; Steven, A. C. *J. Mol. Biol.* **2005**, *348*, 247–252.
(62) Koo, B. W.; Hebda, J. A.; Miranker, A. D. *Protein Eng. Des. Sel.* **2008**, *21*, 147–154.
(63) Nelson, R.; Sawaya, M. R.; Balbirnie, M.; Madsen, A. Ø.; Riekel, C.; Grothe, R.; Eisenberg, D. *Nature* **2005**, *435*, 773–778.

JP9066718